

A multiphase mechanical model for Ti-6Al-4V : application to laser assisted process modeling

Longuet A.^a Robert Y.^{a,b,c} Aeby-Gautier E.^c Appolaire, B.^c Mariage J.F.^b Colin C.^a Cailletaud G.^a

^aCentre des Matériaux, Mines Paristech, CNRS UMR 7633, BP 87, 91003 Evry CEDEX, France

^bCEA Valduc, Laboratoire Calcul et Simulations, 21120 Is-sur-Tille

^cEcole des Mines de Nancy, Parc de Saurupt, 54042 Nancy

Résumé

A multiphase model for Ti-6Al-4V is proposed. This material is widely used in industrial applications and so needs accurate behaviour modeling. Tests have been performed in the temperature range from 25°C to 1020°C and at strain rates between $10^{-3}s^{-1}$ and $1s^{-1}$. That allowed the identification of a multiphase mechanical model coupled with a metallurgical model. The behaviour of each phase is calibrated by solving an inverse problem including a phase transformation model and mechanical model to simulate tests under thermomechanical loadings. A scale transition rule (β -rule) is proposed in order to represent the redistribution of local stresses linked to the heterogeneity of plastic strain. Finally this model is applied to two laser assisted processes : direct laser fabrication and laser welding.

Key words: Ti-6Al-4V, multiphase model, mechanical model, finite element, laser assisted process

PACS:

1. Introduction

Titanium alloys are extensively used in leading industries, due to their low density and high specific strength (Rm/ρ) at elevated temperature (aeronautics, nuclear energy) and their compatibility with human tissues (biomedical applications). The most popular titanium alloy is Ti-6Al-4V (wt%). It has been widely studied by authors. This is a $\alpha + \beta$ type alloy. At room temperature it is mainly composed of HCP α grains with some stabilized BCC β phase. When heated over about 980°C (beta transus), α is totally transformed into β which remains until fusion at about 1660°C. The occurrence of phase transformations leads to changes of microstructures that will involve changes in properties that have to be taken into account in any modelling of the material behaviour during the process. Laser assisted processes involve complex thermal histories, with rapid heating and cooling rates. These rapid thermal evolutions as well as the occurrence of phase changes lead to residual stresses and distortions. This paper is focused on the mo-

deling of two laser processes : laser welding and direct laser fabrication. The main purpose of the calculations is to evaluate the residual stresses and the deformations of the component at the end of the fabrication. The calculation of residual stresses and distortions need to model the coupled thermal metallurgical and mechanical behaviour. Such coupled models have been developed for residual stress calculations of steels or aluminium during quenching or welding [Denis *et al.*, 2002]. In all cases, it is necessary to link the mechanical behaviour to temperature variations and to metallurgical changes, i.e. phase transformations kinetics occurring on heating and cooling. On heating, the transformation occurs mainly by diffusion. Depending on the initial microstructure, the kinetics is mainly governed by the dissolution of the α phase. As β phase is still remaining at room temperature, nucleation step is not necessary. Concerning transformation on cooling from the β temperature range, when the cooling rate is small enough a diffusive transformation occurs, and the β phase transforms back to α , whereas at very high cooling rates a martensitic transformation occurs. The transformation product is called α' . In the studied processes, a large range of temperature and temperature rate is investigated, so that many

Email addresses: arnaud.longuet@ensmp.fr (Longuet A.),
georges.cailletaud@ensmp.fr (Cailletaud G.).

microstructures are present during processing.

A lot of authors have investigated the mechanical behaviour of Ti-6Al-4V at different temperatures and strain rates [Majorell *et al.*, 2002], [Picu et Majorell, 2002], [Robert, 2007], [Vanderhasten *et al.*, 2008], but only a few have linked the microstructure to the mechanical behaviour of the material [Gil *et al.*, 2003]. The aim of this work is to produce a model that takes into account the impact of phase transformation on the mechanical behaviour.

2. Experimental characterization

Laser welding and direct laser fabrication induce high heating and cooling rates, from room temperature to the β domain, and back to room temperature in the area affected by the laser beam. For the rest of the structure, practically no phase change occurs. Considering this, the mechanical properties have to be studied for two kinds of microstructure : the initial microstructure, here a microstructure consisting mainly in globular α phase and β for the material that is not affected by the laser beam (as received material) and the martensitic structure (needle-shape) α' for the deposited or melted material. Three phases have to be considered in the model : α , α' and β . As the β phase is only present at high temperature, the tests are to be done on as received $\alpha + \beta$ Ti-6Al-4V and martensitic α' material. Successive heating and cooling periods produce alternative tension and compression loading, so cyclic behaviour of Ti-6Al-4V has to be investigated. Relaxation tests are needed to characterize the effect of viscosity, and also the static recovery, that is present for slow cooling rates. The material is only considered in its solid state. The shape of the deposited or melted material is considered as known *ex ante*. So the material is heated from room temperature to liquidus (ie : 1660°C). The material model has then to work on the whole temperature range. As a matter of fact, the development of residual stresses occurs when the material becomes solid, so that a special attention is paid for temperature lower than 1000°C. The transition from solid to liquid state is marked by erasing internal stresses and a Norton exponent that becomes equal to 1 (Newton law). The thermal expansion coefficient of Ti-6Al-4V is about $10^{-5} \text{ }^\circ\text{C}^{-1}$, so that the induced thermal strains are lower than 1%. Combining this value with the observed temperature rates, strain rates not exceeding 1s^{-1} are found.

Having in view the domain of validity of the mechanical model, two kinds of tests have been performed :

- strain controlled cyclic tests under symmetric loading ($\pm 1\%$);
- cyclic relaxation tests (60 s dwell time).

Two microstructural states are considered :

- as received material ($\alpha + \beta$) (figure 1);
- martensitic structure obtained after β annealing and water quench (figure 2).

Tests have been performed on an MTS machine equipped with a resistive furnace operating until 950°C in air. The

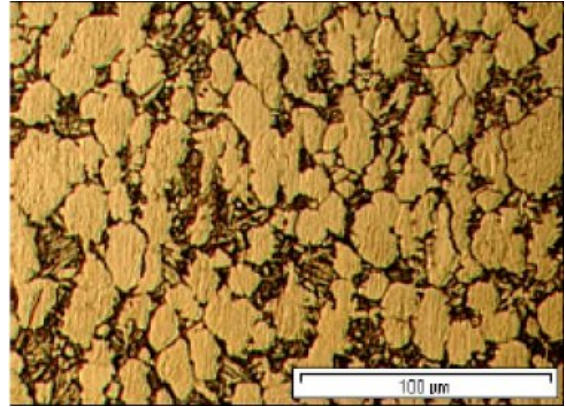


FIG. 1. As received material used for tests

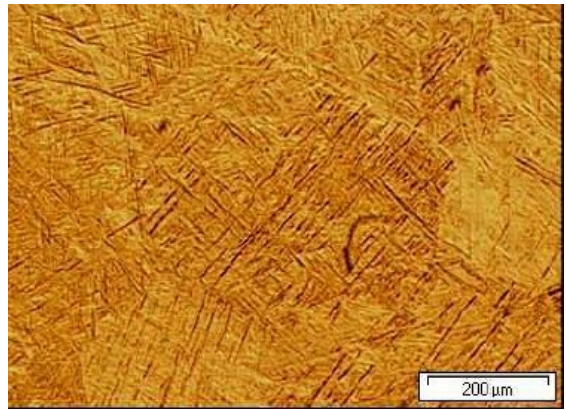


FIG. 2. Martensitic structure used for tests

specimens are taken from plates. The heating rate is about 200°C/h. Incremental cyclic tests have been made, with ten cycles for each step in order to obtain a stabilized loop.

The stability of the material has been proved for constant temperature loadings. This has been made by applying a set of 15 cycles at every 30 minutes, up to 210 minutes. No significant difference is observed between the various loops (only a 3% increase of the maximum stress). That means that no major microstructural evolution (grain growth, diffusion, ...) is present. For the α' structure, ageing may occur during the heating and dwell before the mechanical characterization. Additional tensile tests have been performed at temperatures ranging from 800°C to 500°C on the as quenched microstructure.

Stress relaxation tests have been achieved, with tension and compression periods. Like for the cyclic tests, each test is performed three times to reach stabilized responses. For each temperature (between 20°C and 900°C), four strain rates are prescribed (10^{-5}s^{-1} , 10^{-4}s^{-1} , 10^{-3}s^{-1} , 10^{-2}s^{-1}). The strain amplitude is 1%. Both dwell times are equal to 60 s; at the end of the test, the strain goes back to 0.

3. Material model

3.1. Metallurgical model

The current phase distribution is supposed to be the result of the temperature history $T(\underline{x}, t)$ only. Its evolution is then determined independently in each point. The metallurgical model needs to describe the evolution of the different amounts of each phases (α , α' and β). For titanium alloys, Aluminium is an alpha stabilizing element while Vanadium is a beta stabilizing one. As temperature decreases, the solubility limit of vanadium in the alpha phase is decreasing while it is increasing in the beta phase leading to a phase change at temperatures lower than the T_β temperature. As a consequence, the two equilibrium variables are z_α , the volume fraction of the α phase (poor in vanadium), and z_β , the volume fraction of β phase, enriched in Vanadium. The variable $z_{\alpha'}$ is the volume fraction of α' phase, that is a HCP microstructure, obtained by a martensitic transformation mechanism. Its composition in vanadium is thus the composition of its parent beta phase. It has a typical shape in very thin needles or lamellae. The α' can be produced from the β phase existing at the higher temperatures and rapidly cooled. It has to be mentioned that we consider two different amount fraction of β : a first amount of β of which the chemical composition is the nominal chemical composition of the alloy and the amount of β which has the chemical composition of the previous globular α phase (in case of dissolution of globular α phase during very fast heating prior to any chemical homogeneization).

The volume fraction of β phase, z_β , is computed as $1 - z_\alpha - z_{\alpha'}$. A critical ingredient of the model is the amount of α phase at equilibrium, z_α^{max} , that decreases with temperature, the volume fraction of β phase reaching 1 at 980°C. The phase transformation model [Robert *et al.*, 2006] takes into account the globular α phase, the β phase and the needle-shape α' , that are introduced in a differential system, the equations of which are different for heating and cooling. During heating, the kinetics at which both α and α' phases will tend to the equilibrium is given by the following equations :

$$\dot{z}_\alpha = z_\alpha \frac{z_\alpha^{max^c}(T) - z_\alpha - z_{\alpha'}}{\tau_\alpha(T)} H(T_0 - T) \quad (1)$$

$$+ z_\alpha \frac{z_\alpha^{max^h}(T) - z_\alpha - z_{\alpha'}}{\tau_\alpha(T)} H(T - T_0) \quad (2)$$

$$\dot{z}_{\alpha'} = z_{\alpha'} \frac{z_\alpha^{max}(T) - z_\alpha - z_{\alpha'}}{\tau_{\alpha'}(T)} \quad (3)$$

where $z_\alpha^{max^c}(T)$ describes a diffusion controlled transformation, and $z_\alpha^{max^h}(T)$ characterises a transformation associated to a diffusionless front propagation :

$$z_\alpha^{max^c}(T) = \max(0.925 (1 - e^{-1.25 \cdot 10^{-2}(980-T)}), 0) \quad (4)$$

$$z_\alpha^{max^h}(T) = \max(1 - e^{-0.05 (T_0-T)}, 0) \quad (5)$$

If $z_\alpha^{max}(T) - z_\alpha - z_{\alpha'} \neq 0$ then z_α and $z_{\alpha'}$ will tend to their equilibrium value at a rate proportional to the gap between $z_\alpha^{max}(T)$ and $z_\alpha + z_{\alpha'}$. The kinetics of the phase transformation is driven by $\tau_\alpha(T)$ and $\tau_{\alpha'}(T)$. Due to its morphology and kinetic composition, it is easier for α' to be transformed into β . So $\tau_{\alpha'}(T)$ is smaller than $\tau_\alpha(T)$.

An other diffusion mechanism controls the fact that β takes its equilibrium composition (the corresponding phase is then called β_t) :

$$\dot{z}_{\beta_t} = -z_\beta \frac{z_\beta - z_{\beta_t}}{\tau_t} \quad (6)$$

During cooling, the β_t phase will transform into α' if the temperature is below M_s following Koistinen and Marburger's law. Here, due to the high cooling rates, M_s has been found to be around 800°C, according to free dilatometry tests [Robert, 2007]. At the present, the M_s temperature is taken as the same whatever the composition of the beta phase. The evolution of $\dot{z}_{\alpha'}$ is written as :

$$\dot{z}_{\alpha'} = -z_{\beta_t} \frac{\dot{T}}{\tau_\beta} \quad (7)$$

In both processes diffusion may occur leading to a final microstructure consisting in $\alpha + \beta$ if the material is annealed under β transus [Gil Mur *et al.*, 1996]. In the present case it might be difficult to discriminate between needle-shape α and the α' phase. The model could be improved considering either ageing of martensite or transformation on cooling controlled by diffusion. In the latter case, the cooling rate would be a pertinent variable to make the difference, with a critical value of 570°C/min [Seraphin, 1965]. The mechanical properties of the individual phases will now be considered for the construction of a multiphase model able to dynamically represent the behaviour of the resulting phase mixture.

3.2. Mechanical model

Each phase is assumed to be embedded in the $\alpha + \beta$ mixture, so that it affords a local stress tensor, and will contribute to the deformation of the whole aggregate according to its volume fraction. A “ β —rule” [Cailletaud, 1988, Cailletaud et Pilvin, 1994] is introduced to define the scale transition between the macroscopic level and the level of each phase. For each current phase ϕ ($\phi = \alpha, \beta, \alpha'$), the residual stress is defined by an intergranular accommodation variable $\beta_{\sim\phi}$. The local stress σ_ϕ is then proportional to the difference between $\beta_{\sim\phi}$ and the average of these variables in all phase :

$$\sigma_\phi = \sigma + \mu(\beta_{\sim\phi} - \beta_{\sim\phi}) \quad \text{with} \quad \beta_{\sim\phi} = \sum_{\phi} z_\phi \beta_{\sim\phi} \quad (8)$$

with z_ϕ the volume fraction of each phase ϕ .

The evolution of $\beta_{\sim\phi}$ has a driving term and a dynamic recovery term :

$$\dot{\beta}_{\sim\phi} = \dot{\xi}_{\sim\phi}^p - D_{\phi}\beta_{\sim\phi}\dot{p}_{\phi} \quad (9)$$

where D_{ϕ} is a parameter characterizing the scale transition.

Each phase is described by a viscoplastic model. The local anisotropy due to hexagonal elasticity is neglected. A von Mises criterion is chosen for the viscoplastic model. A kinematic hardening variable is introduced to represent the Bauschinger effect.

On a macroscale, the strain ε is decomposed into several components, the elastic strain, ε^e , the viscoplastic strain, ε^{vp} , the thermal dilatation, ε^{th} and the strain due to phase change, ε^{pc} .

$$\varepsilon = \varepsilon^e + \varepsilon^{vp} + \varepsilon^{th} + \varepsilon^{pc} \quad (10)$$

The elastic strain is related to the macroscopic stress tensor :

$$E\varepsilon^e = (1 + \nu)\sigma - \nu Tr(\sigma)\underline{I} \quad (11)$$

A secant isotropic thermal expansion coefficient is used, so that the thermal dilatation term writes :

$$\varepsilon^{th} = (\alpha(T)(T - T_0) - \alpha(T_{ini})(T_{ini} - T_0))\underline{I} \quad (12)$$

with T the actual temperature, T_{ini} the initial temperature and T_0 the reference temperature at which the coefficient was measured.

The strain due to phase change represents the specific volume variation between HCP and BCC networks. The HCP phase (the most compact) is taken as reference, so that ε^{pc} is proportional to the volume fraction z_{β} :

$$\varepsilon^{pc} = \delta_{\alpha \rightarrow \beta} z_{\beta} \underline{I} \quad (13)$$

where $\delta_{\alpha \rightarrow \beta}$ is one third of the specific volume variation.

Each phase is affected a yield function

$$f_{\phi} = J(\sigma_{\phi} - \underline{X}_{\phi}) - \sigma_{y\phi} \quad (14)$$

with $\sigma_{y\phi}$ the initial yield stress of phase ϕ and J the second von Mises invariant which is written :

$$J(\sigma_{\phi} - \underline{X}_{\phi}) = \sqrt{\frac{3}{2}(\underline{s}_{\phi} - \underline{X}_{\phi}) : (\underline{s}_{\phi} - \underline{X}_{\phi})} \quad (15)$$

A viscoplastic potential is built from f_{ϕ} . The viscoplastic strain rate in the phase is equal to its derivative with respect to local stress tensor :

$$\Omega_{\phi} = \frac{n_{\phi} + 1}{K_{\phi}} \left\langle \frac{f_{\phi}}{K_{\phi}} \right\rangle^{n_{\phi} + 1} \quad (16)$$

$$\dot{\xi}_{\phi}^p = \frac{\partial \Omega_{\phi}}{\partial \sigma_{\phi}} = \frac{\partial \Omega_{\phi}}{\partial f_{\phi}} \frac{\partial f_{\phi}}{\partial \sigma_{\phi}} \quad (17)$$

The direction of the viscoplastic flow and its intensity are then given by :

$$\frac{\partial f_{\phi}}{\partial \sigma_{\phi}} = n_{\phi} = \frac{3}{2} \frac{\underline{s}_{\phi} - \underline{X}_{\phi}}{J(\sigma_{\phi} - \underline{X}_{\phi})} \quad (18)$$

$$\dot{p}_{\phi} = \frac{\partial \Omega_{\phi}}{\partial f_{\phi}} = \left(\frac{f_{\phi}}{K_{\phi}} \right)^{n_{\phi}} \quad (19)$$

so that, finally :

$$\dot{\xi}_{\phi}^p = \dot{p}_{\phi} n_{\phi} \quad (20)$$

The evolution rule of the kinematic hardening variable involve a dynamic recovery term and a static recovery term :

$$\dot{\alpha}_{\phi} = \dot{\xi}_{\phi}^p - d_{\phi} \alpha_{\phi} \dot{p}_{\phi} - \left(\frac{J(\alpha_{\phi})}{M_{\phi}} \right)^{m_{\phi}} \frac{\alpha_{\phi}}{J(\alpha_{\phi})}$$

with $J(\alpha_{\phi}) = \sqrt{\frac{2}{3}} \alpha_{\phi} : \alpha_{\phi}$ and $\underline{X}_{\phi} = \frac{2}{3} C_{\phi} \alpha_{\phi}$ (21)

A set of cyclic and relaxation tests from room temperature to 1050°C have been done [Robert *et al.*, 2006]. They include a series of tests on various microstructures, and allow the calibration of the various material parameters. Between 1050°C and 2500°C, an extrapolation has been made [Robert, 2007], since Ti-6Al-4V becomes too soft to be tested.

4. Results and discussion

4.1. Application of the multiphase model

The identification of the model is performed in several steps. Each metallurgical phase has its own thermomechanical properties. To begin with, the model is fitted for each temperature tested without the scale transition rule, in order to get a first approximation of the parameters. Some of the parameters are not temperature dependent (for instance d_{ϕ} in the kinematic hardening rule). For the other ones, a temperature dependent function is introduced to get the best fit with respect to temperature. The final identification is made by computing the whole life of the specimen : starting from the initial phase distribution, the metallurgical model allows to predict the volume fraction of each phase during the test. Depending on the initial temperature history, the specimens have a different amount of each phase. This provides us with a series of different cases with various phase amounts. A typical result is shown in figure 3, that shows the comparison between experiments and simulation at 800°C for different strain rates. A good agreement at high temperatures is critical for the model to be realistic and to be able to model the manufacturing processes. This is why the mechanical response of the model is checked on the whole temperature range.

The behaviour is time insensitive (elastoplastic) from room temperature to 550°C : the values of n and K have then been chosen to give a low viscous stress. When the temperature becomes higher, the elastoplastic stress component decreases whereas the viscoplastic part raises (see figure 4). The transition is found around 550°C. The highest viscous stress is obtained around 800°C (figure 4). In

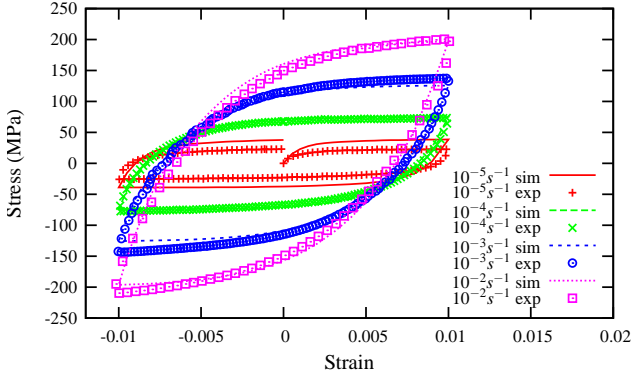


FIG. 3. Comparison between experiment and simulation at 800°C for different strain rates for the $\alpha + \beta$ structure

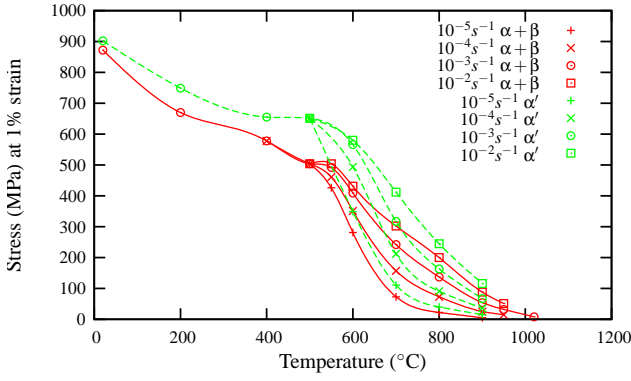


FIG. 4. Stress at 1% strain with respect to temperature for different strain rates

any case, the maximum stress decreases when the temperature increases. Figure 5 shows the evolution of the yield stress $\sigma_{0.2}$ versus temperature in each phase for an intermediate strain rate of 10^{-2} s^{-1} . The curve is obtained by means of the following analytic expression :

$$\sigma_{0.2\phi} = \sigma_{y\phi} + \frac{C_\phi}{d_\phi} (1 - e^{-d_\phi \epsilon_\phi^p}) + K_\phi (\dot{\epsilon}_\phi)^{\frac{1}{n_\phi}} \quad (22)$$

For high temperatures (more than 1000°C) the stress level tends to zero for the strain rates of interest in our simulations. There is a little difference between the experimentally measured stress in figure 4 and the simulated results in figure 5. This is due to the static recovery term that is not taken into account in the simplified expression (eq.22).

Figure 5 sorts the different phases by their yield stress. The martensitic structure has the highest stress at low temperature, which is in good agreement with literature [Majorell *et al.*, 2002]. The β phase has a higher stress than α and α' at high temperature. First this phase is only present from 700°C to liquidus and its proportion exceeds 50% only over 900°C. Thus, for temperatures under 900°C the behaviour of the β phase only has a little influence on the global behaviour of the material. Finally for temperatures over 900°C the obtained stresses are very low, that explains the results shown in figure 5.

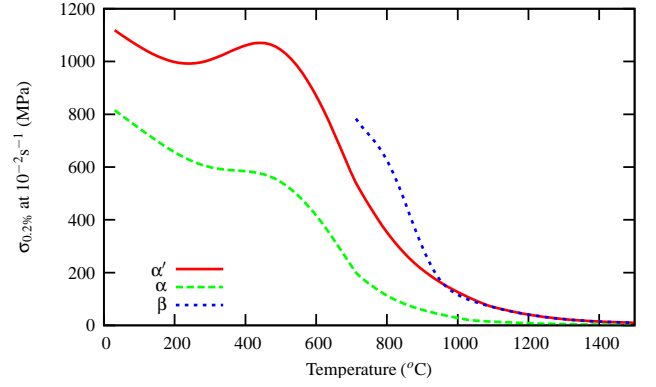


FIG. 5. Stress at 0.2% strain and a strain rate of 10^{-2} s^{-1} for each phase

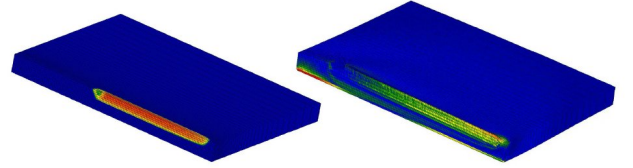


FIG. 6. Von Mises stress (right) and amount of α' phase (left) during welding of Ti-6Al-4V sheets

4.2. Process simulation

The model is implemented in the finite element code ZéBuLoN [Besson *et al.*, 1998]. This allows us to model industrial processes like laser welding and direct laser fabrication. In both cases, two finite element computations are performed. The temperature field is first evaluated. Taking the temperature history as an input, a metallurgico-mechanical computation is made. The final result is the spatial distribution of the phases, the residual stress field and the distortion of the component.

In the laser welding process, the laser beam moves along the join and shots shorts pulses that create a molten pool. There is no heating of the component, but in the small affected zone. The duration of the pulses is in a 1–20 ms range, so that there is a cyclic loading for the material points situated on the path of the beam. Figure 6 shows the result of the numerical simulation of the welding between two sheets made of Ti-6Al-4V. The test has been made at CEA Valduc [Robert, 2007]. At the end of the welding, the assembly has a V-shape, due to the contraction in the area of the weld bead. The initial structure of the material was $\alpha + \beta$. There is a marked phase transformation in a small area near the junction, from the initial structure to pure β , then to α' during the subsequent cooling. The trace of the beam can then be seen on the specimen (contour map on the left in figure 6). The contour map on the right of the same figure shows the shape of the von Mises stress field at the end of the process. The residual stresses correspond to a bending profile, localized to the area of the weld bead. The experimental value of the deflection is 0.280 mm; the prediction resulting from the whole numerical procedure is 0.200 mm.

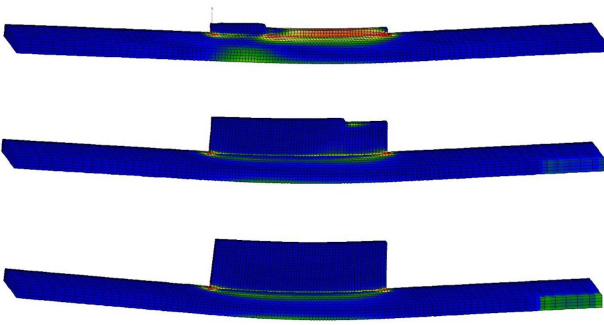


FIG. 7. Evolution of the von Mises stress field and of the substrate deflection during the manufacturing of a wall by direct laser deposition at different time steps (strains $\times 5$)

The direct laser fabrication is much more complicated. The simulation of the process needs to account for the regular addition of material. The metallic powder is thrown on the substrate and melted in the molten pool by the co-axial laser beam. The thickness of the deposited layer is a few hundreds of micrometers, and the diameter of the laser beam is about 2 mm. The process modelling is obtained in the simulation by a specific procedure that “activates” the elements of an initially empty mesh. The appearance of the material is represented by an abrupt change of the thermal and mechanical properties : the element becomes able to conduct heat, and stiff. A questionable point in the procedure is the initial temperature in the element when the material takes its new status. This data include a series of very complex phenomena, including the rapid evolution of the drop after the contact. The value chosen in the simulation shown in figure 7 is 1200°C. The three contour plots show the progressive deformation of the substrate when the “wall” height increases. Even if the strains remain moderate, the displacement of the plate is large enough. A deflection of 1.2 mm has been measured on the specimen at the end of the process (the test has been performed at the Gerailp). The numerical simulation provides a value of 1 mm.

5. Concluding remarks

The multiphase model developed for Ti-6Al-4V is valid for a wide range of temperature and strain rates. It captures the role of $\alpha + \beta$ and α' phases and also the relaxation and the viscosity of the material. It remains enough manageable to be used in pre-industrial finite element computations. It has been successfully applied to the modelling of laser welding and of direct laser fabrication.

Références

[Besson *et al.*, 1998] BESSON, J., LE RICHE, R., FOERCH, R. et CAILLETAUD, G. (1998). Object-oriented programming applied to the finite element method. Part II : Application to material behaviors. *Revue Européenne des Éléments Finis*, 7(5):567–588.

[Cailletaud, 1988] CAILLETAUD, G. (1988). Une approche micromécanique du comportement plastique des polycristaux. *Revue de Physique Appliquée*, 23:353–365.

[Cailletaud et Pilvin, 1994] CAILLETAUD, G. et PILVIN, P. (1994). Utilisation de modèles polycristallins pour le calcul par éléments finis. *Revue Européenne des Éléments Finis*, 3(4):515–541.

[Denis *et al.*, 2002] DENIS, S., ARCHAMBAULT, P. et GAUTIER, E. (2002). Prediction of residual stress and distortion of ferrous and non-ferrous metals : Current status and future developments. *Journal of Materials Engineering and Performance*, 11(1):92–102.

[Gil *et al.*, 2003] GIL, F., MANERO, J., GINEBRA, M. et PLANELL, J. (2003). The effect of cooling rate on the cyclic deformation of β -annealed Ti-6Al-4V. *Material Science and Engineering*, 349:150–155.

[Gil Mur *et al.*, 1996] GIL MUR, F., RODRIGUEZ, D. et PLANELL, J. (1996). Influence of tempering temperature and time on the α' Ti-6Al-4V martensite. *Journal of Alloys and Compounds*, 234:287–289.

[Majorell *et al.*, 2002] MAJORELL, A., SRIVATSA, S. et PICU, R. (2002). Mechanical behavior of Ti-6Al-4V at high and moderate temperature – part I experimental results. *Material Science and Engineering*, 326:297–305.

[Picu et Majorell, 2002] PICU, R. et MAJORELL, A. (2002). Mechanical behavior of Ti-6Al-4V at high and moderate temperature – part II : constitutive modeling. *Material Science and Engineering*, 326:306–316.

[Robert, 2007] ROBERT, Y. (2007). *Simulation numérique du soudage du TA6V par laser YAG impulsif : caractérisation expérimentale et modélisation des aspects thermomécaniques associés à ce procédé*. Thèse de doctorat, École Nationale Supérieure des Mines de Paris.

[Robert *et al.*, 2006] ROBERT, Y., MARIAGE, J.-F., CAILLETAUD, G. et AEBY-GAUTIER, E. (2006). Modélisation numérique du procédé de soudage par laser YAG impulsif d’un alliage de titane (TA6V). In *Matériaux 2006*, Dijon, France.

[Seraphin, 1965] SERAPHIN, L. (1965). Réponse des alliages de titane aux traitements thermiques. *Mémoires scientifiques de la revue de métallurgie*, 62:291–304.

[Vanderhastén *et al.*, 2008] VANDERHASTEN, M., RABET, L. et VERLINDEN, B. (2008). Ti-6Al-4V : Deformation map and modelisation of tensile behaviour. *Materials and Design*, 29:1090–1098.